ACS SENSORS

Article

Cite This: ACS Sens. 2020, 5, 65−72

pubs.acs.org/acssensors

Optical Biosensor for Rapid Detection of *Salmonella typhimurium* Based on Porous Gold@Platinum Nanocatalysts and a 3D Fluidic Chip

Lingyan Zheng, Gaozhe Cai, Wuzhen Qi, Siyuan Wang, Maohua Wang, and Jianhan Lin*

Key Laboratory of Agricultural Information Acquisition Technology, Ministry of Agriculture and Rural Affairs, China Agricultural University, Beijing 100083, China

Supporting Information

ABSTRACT: Screening of pathogenic bacteria is a key to avoid food poisoning. The major drawbacks of existing assays for foodborne bacteria detection include long time for culture, complex DNA extraction for the polymerase chain reaction (PCR), and low sensitivity for enzyme-linked immunosorbent assay (ELISA), greatly limiting their practical applications. Here, we developed a sensitive optical biosensor based on porous gold@platinum nanocatalysts (Au@PtNCs) and a passive three-dimensional (3D) micromixer for fast detection of *Salmonella typhimurium*. The target *Salmonella* cells were first separated using immunomagnetic nanoparticles and the passive 3D micromixer. Then, immune Au@PtNCs were labeled onto the target cells as signal output to catalyze hydrogen peroxide−3,3′,5,5′-tetramethylbenzidine. Finally, the absorbance was measured at 652 nm to calculate the bacterial amount. This optical biosensor could detect *Salmonella* at concentrations from 1.8×10^1 to 1.8×10^7 CFU/mL in 1 h. Its detection limit was calculated to be 17 CFU/mL. Besides, this passive 3D micromixer could magnetically separate 99% of target bacteria from the sample in 10 min. This biosensor has the potential to be extended to detect other bacteria by changing the antibodies.

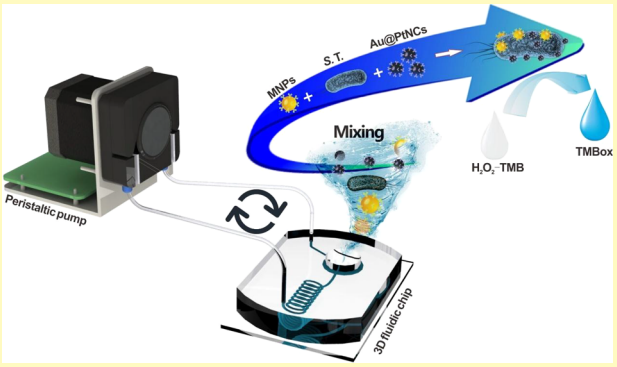

KEYWORDS: *optical biosensor, porous gold@platinum nanocatalyst, passive 3D micromixer, magnetic separation, Salmonella detection*

INTRODUCTION

Food safety is now faced with enormous challenges and has attracted increasing concerns globally.[1] Foodborne diseases due to microbial, parasitic, and chemical contaminations have caused considerable economic losses and become a growing public health issue.[2,3] Since many pathogenic bacteria have low infectious dose (e.g., infectious dose for *Salmonella* is 10^3 CFU/mL),[4] screening of bacteria contaminated foods is crucial to prevention of food poisoning. Existing detection methods, such as gold standard culture and polymerase chain reaction (PCR), either are time-consuming or need professional operations and expensive instruments.[5,6] In recent years, various immunoassays were developed to detect different foodborne bacteria. Among them, enzyme-linked immunosorbent assay (ELISA) is often used for food analysis and clinical diagnostics because it features high throughput, fast detection, and automatic operation.[7,8] However, its insufficient sensitivity (detection limit: ~10^4 CFU/mL) could not meet the requirement for *Salmonella* detection due to inefficient solid−liquid reaction between the antibodies and the target bacterial cells and hard labeling of natural enzymes onto the antibodies.[6,7,9] Thus, it is urgently needed to develop fast, sensitive, and simple bacterial detection methods.

To date, rapid screening of foodborne bacteria has been a big challenge because of complex food background and few target bacteria in food samples.[10] Over the past decades, many efforts on biological signal enhancement have been made to improve the sensitivity of various biosensors.[5,11−18] Compared to natural enzymes that are often reported to amplify biological signals, many nanocatalysts have been developed with features of low cost, good stability, and excellent catalytic activity, and applied in the development of biosensors.[19−21] For example, graphene quantum dots (GQDs) were successfully used as a peroxidase mimic to develop electrochemical biosensors for detection of *Yersinia enterocolitica*[22] and carcinoembryonic antigen.[23] Besides, porous gold@platinum nanocatalysts (Au@PtNCs) have also attracted increasing attention since their three-dimensional (3D) porous structures feature higher specific surface area, better molecular accessibility, and more catalytic active sites.[24,25] Meanwhile, Au@PtNCs have been found to possess similar enzymatic activity to natural

Received: August 3, 2019
Accepted: December 25, 2019
Published: December 25, 2019

DOI: 10.1021/acssensors.9b01472
ACS Sens. 2020, 5, 65−72

peroxidases and are promising in replacing currently available expensive natural enzymes in practical applications.[26−28]

In the past decade, microfluidic chips have often been reported by researchers in the development of biosensors for biochemical analysis, clinical diagnosis, and food safety testing due to their miniaturization, integration, and automation.[29,30] A typical study on a microfluidic biosensor was reported by Lim using quantum dot labeling to rapidly detect pathogenic *Salmonella*, which could detect *Salmonella* in 1 h with a detection limit of 10^3 CFU/mL. However, it had some limitations, such as complex operation and high pressure.[31,32] In the development of microfluidic biosensors, micromixers, the key component of microfluidic chips, play an important role since their mixing efficiency has a great impact on the immune reaction between the antibodies and the antigens and the catalytic reaction between the enzymes and the substrates in the regime of laminar flow.[33,34] To improve the mixing efficiency of micromixers, various microstructures were developed to enhance the mixing of the fluids in microfluidic chips.[32] Among these structures, 3D structures for passive mixing are receiving increasing attention due to their high mixing efficiency and nonexternal power requirement. An interesting study on fabrication of complex 3D structures was reported by Velders using a 3D printer with acrylonitrile butadiene styrene (ABS) to fabricate an ABS channel mold, followed by casting the channel mold with poly(dimethylsiloxane) (PDMS) and dissolving the ABS mold with acetone to obtain the 3D channel.[35]

Here, we developed a sensitive and enzyme-free optical biosensor based on porous gold@platinum nanocatalysts and a passive 3D micromixer for fast and semiautomatic detection of *Salmonella*. As illustrated in Scheme 1, *Salmonella* was first separated specifically using monoclonal antibody-coated magnetic nanoparticles (immune MNPs) in the 3D fluidic chip, resulting in the formation of MNP−bacteria complexes (magnetic bacteria). Then, polyclonal antibody-coated Au@PtNCs (immune Au@PtNCs) were employed to label the magnetic bacteria, leading to the formation of MNP−bacteria−Au@PtNC complexes (nanocatalyst bacteria). After washing to remove the excessive Au@PtNCs, the nanocatalyst bacteria were used for catalysis of hydrogen peroxide−3,3′,5,5′-tetramethylbenzidine (H_2O_2−TMB), and a colored catalysate was produced. Finally, the catalysate was measured using a microplate reader, and its absorbance at 652 nm was used to calculate the amount of target bacteria.

Scheme 1. (a) Schematic for the Synthesis of Porous Gold@Platinum Nanocatalysts; (b) Schematic of the Optical Biosensor for Detection of *Salmonella typhimurium*

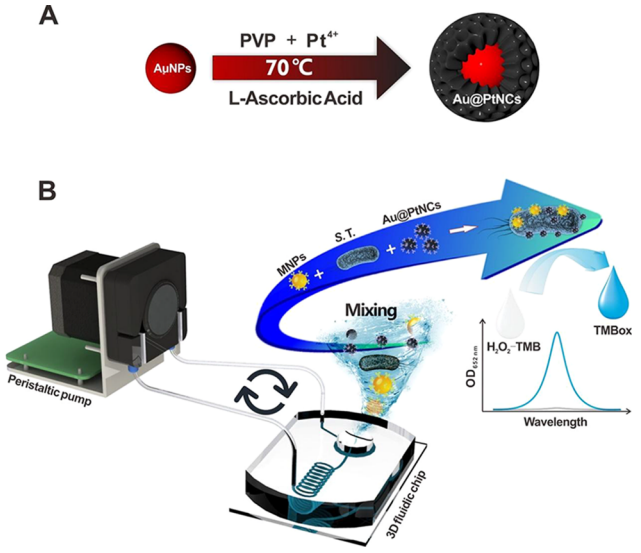

MATERIALS AND METHODS

Materials. *S. typhimurium* was used as a research model, and *Vibrio parahaemolyticus*, *Bacillus cereus*, *Staphylococcus aureus*, *Listeria monocytogenes*, and *Escherichia coli* O157:H7 were used as nontargets. Anti-*S. typhimurium* monoclonal antibodies (1 mg/mL) from Meridian (Cincinnati, OH) and anti-*S. typhimurium* polyclonal antibodies (2.8 mg/mL) from Fitzgerald (Acton, MA) were employed to specifically react with *S. typhimurium*. Gold(III) chloride trihydrate ($HAuCl_4{\cdot}3H_2O$), chloroplatinic acid ($H_2PtCl_6{\cdot}6H_2O$), and poly(vinylpyrrolidone) (PVP, 10 kDa) from Sigma (Saint Louis, MO) were used with trisodium citrate and ascorbic acid (Aladdin, Shanghai, China) to synthesize gold nanoparticles (AuNPs) and Au@PtNCs. Streptavidin-coated magnetic nanoparticles (concentration: ∼1 mg/mL, size: 150 nm) from Ocean Nanotech (Dunedin, FL) were employed to magnetically and specifically separate *S. typhimurium*. Bovine serum albumin (BSA) from Sigma was used for blocking. H_2O_2−TMB and horseradish peroxidase (HRP) were purchased from Solarbio (Beijing, China). Brain heart infusion (BHI) and Lysogeny broth (LB) medium were purchased from Remel (Lenexa, KS) and Aoboxing (Beijing, China), respectively, and used to culture bacteria. Acrylonitrile butadiene styrene and a silicone elastomer kit were used for fabrication of the 3D spiral fluidic channel, which was bonded with a glass slide to develop the fluidic chip. Deionized water from Millipore Advantage (18.2 MΩ cm, Billerica, MA) was used to prepare the solutions.

Synthesis of the Porous Gold@Platinum Nanocatalysts. The porous gold@platinum nanocatalyst is a key material for the fabricated biosensor. Prior to the synthesis of the nanocatalysts, gold nanoparticle seeds were synthesized according to a previously reported hydrothermal reduction method to obtain AuNPs with a size of ∼15 nm and a concentration of ∼19 nM.[36−38]

Au@PtNCs were synthesized based on a reported protocol with some modifications.[26] First, 31 μL of AuNP seeds (diluted two times to 10 nM) were dispersed into 969 μL of deionized water and mixed with 20 μL of PVP (20 wt %) for 5 min under vigorous stirring. Then, 60 μL of 100 mM H_2PtCl_6 and 40 μL of 100 mg/mL ascorbic acid were added and heated to 70 °C for 30 min, until the color changed from red to black. This indicated successful synthesis of Au@PtNCs. After the resulting Au@PtNCs were cooled down to room temperature and residuals were discarded by centrifugation (3000*g*, 10 min) at 4 °C, the Au@PtNCs were finally dissolved by 1.0 mL of deionized water and stored at 4 °C. The size of the Au@PtNCs ranging from 26 to 101 nm was controlled using different amounts of H_2PtCl_6.

Preparation of the Immune Au@PtNCs. The Au@PtNCs were coated with polyclonal detection antibodies based on reported studies with some modifications.[26,28] First, 200 μL of the synthesized Au@PtNCs were added into 1.0 mL of phosphate buffered solution (PBS, 0.01 M, pH 7.2) and mixed with 15 μg of the detection antibodies, followed by incubation at 37 °C for 3.5 h under gentle shaking. Then, 200 μL of β-casein (20 wt %) in PBS was added to incubate at 37 °C for 90 min for blocking the excessive sites on the surface of Au@PtNCs. Finally, the immune Au@PtNCs were collected by centrifugation (2500*g*, 10 min) at 4 °C and dispersed in 200 μL of PB containing 10% sucrose, 1.0% BSA, 1.0% PVP, and 1% β-casein.

Fabrication of the 3D Fluidic Chip. The 3D fluidic chip is a key to the biosensor and was fabricated using the ABS scaffold removal method. The 3D fluidic chip mainly includes two parts: (1) an open cylinder mixer (radius: 0.5 cm, height: 1 cm) for rapidly mixing the target bacterial sample with the immune MNPs and the immune Au@PtNCs, and (2) a spiral incubator (radius: 0.5 mm, turn: 10) for

DOI: 10.1021/acssensors.9b01472
ACS Sens. 2020, 5, 65−72

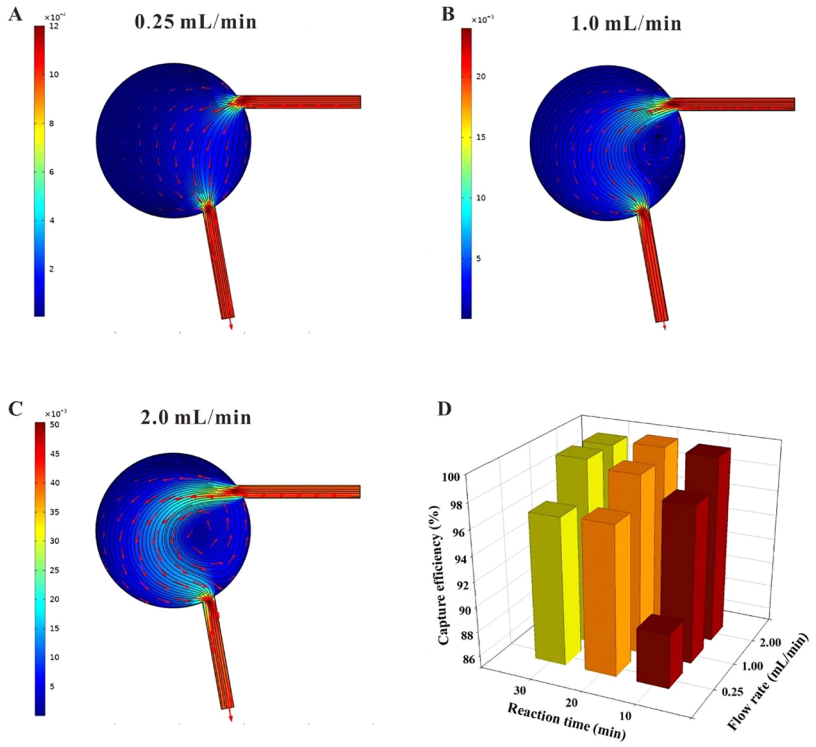

Figure 1. (A) Vortex effect of the mixer at 0.25 mL/min; (B) the vortex effect of the mixer at 1.0 mL/min; (C) the vortex effect of the mixer at 2.0 mL/min; (D) the capture efficiency of the target bacteria at different flow rates and reaction times.

allowing sufficient binding of the target bacterial cells with the MNPs and the Au@PtNCs. The angle between the inlet and the outlet of the mixer was selected to be 60° based on previous reports.[34,39]

The ABS mold of the 3D spiral channel was first printed using a 3D printer and cast by a mixture of the prepolymer and the curing agent (mass ratio = 10:1), followed by curing at 65 °C for 12 h. Then, the PDMS channel was immersed in acetone for 24 h to dissolve the ABS mold, leading to the formation of the 3D channel. After rinsing with deionized water and drying by air flow, the 3D spiral PDMS channel was cleaned using surface plasmons (Harrick Plasma, Ithaca, NY) and finally bonded onto a glass slide to form the fluidic chip.

Calibration Model of the Proposed Biosensor. To build the calibration model, different concentrations (1.8×10^1–1.8×10^7 CFU/mL) of the target bacterial samples were detected using the biosensor. Prior to tests, 1 mL of 1% BSA (10 mg/mL) was used to block the fluidic chip for 30 min to avoid nonspecific protein adsorption, followed by washing with PBST (PBS containing 0.5% Tween-20). First, 500 μL of the bacterial sample was added into the cylinder mixer through open windows, and a peristaltic pump (WX10, Longer Pump, Baoding, China) was connected with the inlet and outlet of the fluidic chip, respectively, to recycle the sample at 2 mL/min. Then, 20 μL of the immune MNPs were added drop by drop, allowing the MNPs to specifically capture the target bacterial cells for 10 min for forming the magnetic bacteria, followed by addition of 15 μL of the immune Au@PtNCs drop by drop into the mixer and recycling for 30 min, resulting in the formation of the nanocatalyst bacteria. After the nanocatalyst bacteria were flushed out at the same flow rate of 2 mL/min, they were washed with PBST twice on a magnetic separator (SMS0206, Aibit, Wuxi, China) to remove the excessive Au@PtNCs. The nanocatalyst bacteria were finally dissolved in 200 μL of H_2O_2–TMB and incubated at 37°C for 15 min, and the catalysate was analyzed using an Infinite M200 reader (Tecan, Austria). The absorption at 652 nm was plotted with the bacterial amount to obtain the calibration model of the biosensor.

Detection of *Salmonella* in Spiked Samples. To demonstrate the applicability of the biosensor in real food samples, the samples were prepared according to food safety national standards in China. First, 25 g of chicken meat was homogenized with 225 mL of PBS solution in a Stomacher bag through a BagMixer (InterScience, Paris, France). After standing for 10 min, the supernatant was taken out. Different amounts of pure *Salmonella* cells were then spiked to obtain the mimic real samples containing target bacteria at concentrations of 5.7×10^1–5.7×10^3 CFU/mL. The prepared samples were finally tested using the biosensor.

RESULTS AND DISCUSSION

Simulation and Optimization of the 3D Fluidic Chip. Rapid and efficient mixing in a small-sized channel is a challenge due to the very small Reynolds number, indicating a regime of laminar flow in the channel.[39] In this study, a passive 3D mixer was developed and simulated using COMSOL. More details on the simulation could be found in the Supporting Information. As shown in Figure 1A–C, when the flow rate was increased to 2.00 mL/min, the vortexing increased obviously, indicating that two fluids could be mixed more uniformly. This could also be observed from Video S1 in the Supporting Information. To verify this, the immune MNPs and the target bacteria were used at different flow rates and reaction times in the 3D fluidic chip, and the capture efficiency of the target bacteria (ratio of separated bacteria to original bacteria) was employed to evaluate the mixer. As shown in Figure 1D, when the flow rate was changed from 0.25 to 2.00 mL/min and the reaction time was changed from 10 to 30 min, the capture efficiency changed from 89.4 to 99.60%. To establish a trade-off between the time and capture efficiency, the optimal flow rate of 2.00 mL/min and reaction time of 10 min were used in this study. To further verify the effect of this passive micromixer, the immune MNPs and the target bacteria were used at the same reaction time and with different mixing methods: vortexing, shaking, and the proposed 3D mixing. Figure S1 shows that the capture efficiency of *Salmonella* was ~98.5%, which was obviously higher than those for shaking

DOI: 10.1021/acssensors.9b01472
ACS Sens. 2020, 5, 65–72

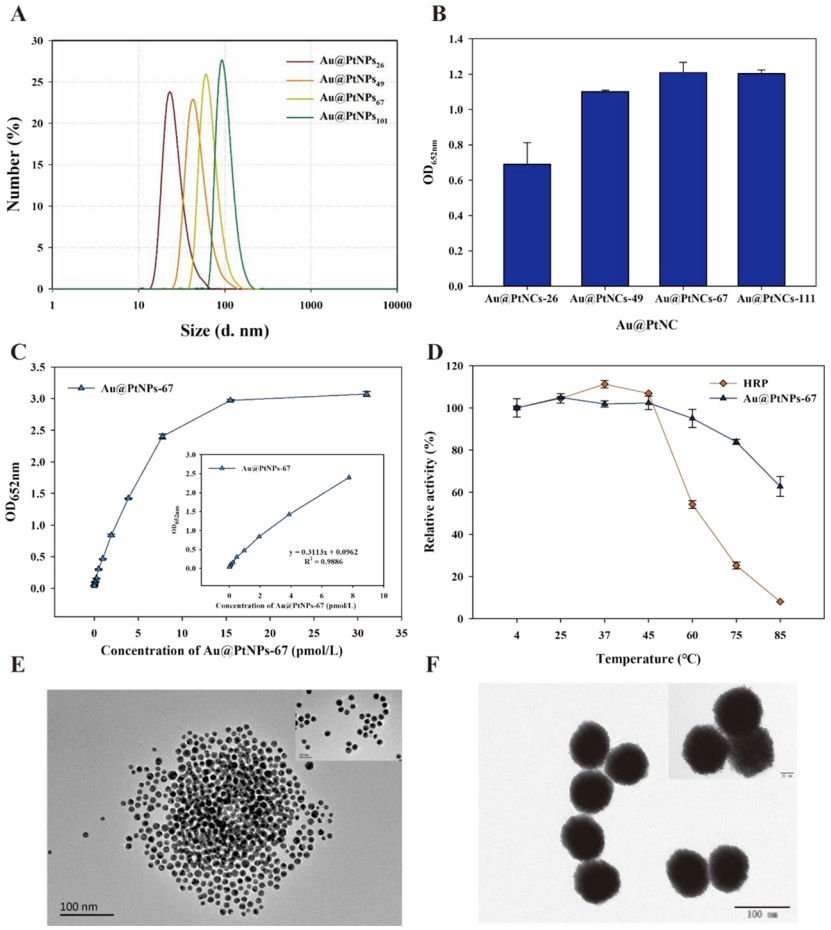

Figure 2. (A) DLS results for different sizes of the Au@PtNCs; (B) comparison of catalytic activity for different sizes of Au@PtNCs; (C) the absorbance for different concentrations of Au@PtNCs to catalyze the H_2O_2−TMB substrate; (D) catalytic activity comparison of the Au@PtNCs and HRP at different temperatures; (E, F) transmission electron microscopy (TEM) images of the AuNPs and Au@PtNCs.

(75.7%) and vortexing (44.1%), and the absorption of *Salmonella* at 6.3 × 10^3 CFU/mL for the 3D mixing was 0.64, which was much higher than those for shaking (0.48) and vortexing (0.31). The higher capture efficiency and absorption demonstrated that the proposed passive 3D micromixer had superior mixing efficiency over shaking and vortexing.

Characterization of the Immune Au@PtNCs. The biosensor relied on mimic enzymatic characteristics of the Au@PtNCs. Different sizes of porous Au@PtNCs were synthesized using the seed-mediated growth method and characterized using dynamic light scattering (DLS). Figure 2A shows the DLS data for different sizes (26, 49, 67, and 101 nm) of the Au@PtNCs. The DLS results indicated that the polydispersity indices (PDIs) for Au@PtNCs-26, Au@PtNCs-49, Au@PtNCs-67, and Au@PtNCs-101 were 0.279, 0.171, 0.064, and 0.030, respectively, indicating that the synthesized Au@PtNCs exhibited good monodispersity. To achieve the highest sensitivity, these Au@PtNCs (concentration: 3 pmol/L) were all employed for catalysis of a H_2O_2−TMB substrate. Figure 2B shows that the absorbance of Au@PtNCs-67 and Au@PtNCs-101 was obviously larger than that of Au@PtNCs-26 and Au@PtNCs-49. Since the smaller size of Au@PtNCs imparted better water solubility, the Au@PtNCs with a size of 67 nm were selected as the optimal signal output and used in this study.

The biosensor was developed based on the intrinsic peroxidase mimic of the Au@PtNCs. Thus, different concentrations of the Au@PtNCs were employed to catalyze H_2O_2−TMB. Figure 2C shows that the absorbance at 652 nm increased with Au@PtNC concentration, and a good linear relationship between absorbance and concentration from 0.0038 to 7.75 pmol/L was found. Another advantage of the Au@PtNCs over HRP is their high temperature tolerance. To verify this, both Au@PtNCs and HRP were used to catalyze the H_2O_2−TMB substrate at different temperatures from 4 to 85 °C. As shown in Figure 2D, the Au@PtNCs had comparable catalytic activity with HRP when the temperature was lower than 45 °C. However, when the temperature kept increasing, the activity of HRP dropped very quickly to 8.06% at 85 °C, and that of the Au@PtNCs decreased much slowly and still reached up to 62% at 85 °C, indicating that the Au@PtNCs had much better high temperature tolerance than HRP.

Besides, transmission electron microscopy (TEM) and UV−vis absorption spectroscopy were conducted to verify successful synthesis of the AuNPs and Au@PtNCs. As shown in Figure 2E,F, the AuNPs and Au@PtNCs with a uniform size of ∼67 nm were successfully synthesized and well monodispersed. The absorption spectra are shown in Figure S2. The AuNPs displayed a strong optical absorption peak near 520 nm, while the absorption peak of the Au@PtNCs disappeared, indicating that the Au@PtNCs were synthesized successfully.

To further verify the successful modification of the detection antibodies onto the Au@PtNCs, both DLS analysis and

DOI: 10.1021/acssensors.9b01472
ACS Sens. 2020, 5, 65−72

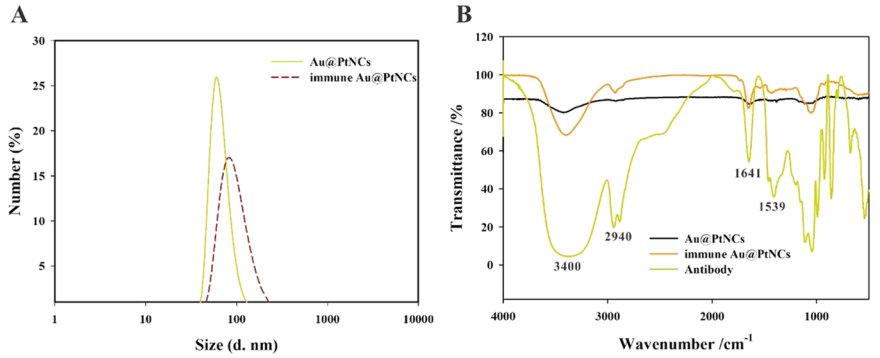

Figure 3. (A) DLS results for the Au@PtNCs and the immune Au@PtNCs; (B) FTIR results for the Au@PtNCs, the detection antibodies, and the immune Au@PtNCs.

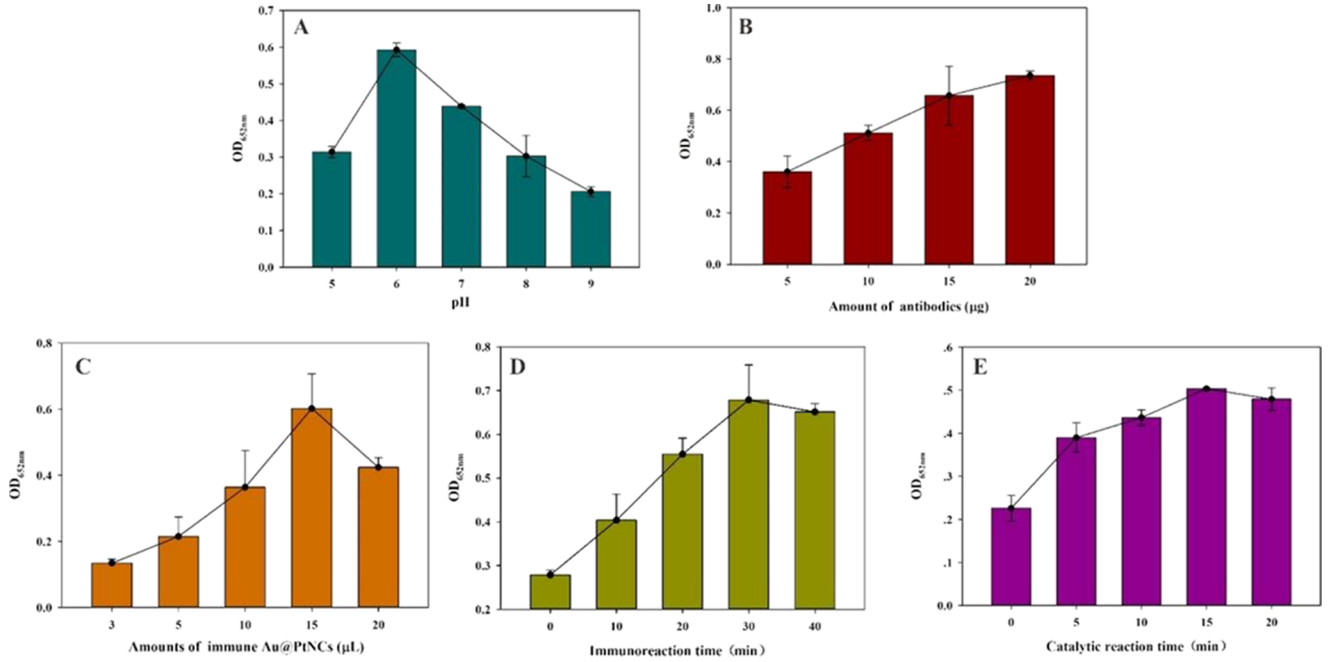

Figure 4. Optimization of the biosensor: (A) optimization of the pH value for modification of detection antibodies onto Au@PtNCs; (B) optimization of the amount of detection antibodies for preparation of immune Au@PtNCs; (C) optimization of the amount of immune Au@PtNCs; (D) optimization of the time for immunoreaction between antibodies and target bacteria; (E) optimization of the catalysis time for Au@PtNCs to catalyze H_2O_2−TMB.

Fourier transform infrared (FTIR) spectroscopy were performed. Figure 3A shows that the DLS results indicated that the size of the Au@PtNCs increased from 67 to 83 nm after the Au@PtNCs were modified with the detection antibodies, indicating the successful modification of the antibodies onto the Au@PtNCs. The FTIR spectra of the Au@PtNCs, the detection antibodies, and the immune Au@PtNCs are shown in Figure 3B. The spectra of the Au@PtNCs did not exhibit obvious characteristic peaks, except for a small peak at 3400 cm^{-1} (COO−H). As is well known, proteins and peptides have obvious infrared characteristic peaks at around 1650 and 1550 cm^{-1}.[28] Thus, the peptide bond characteristic peaks at 1539.19 cm^{-1} (N−C═O) and 1641.88 cm^{-1} (C═O) were found in the spectra of immune Au@PtNCs and detection antibodies and not present in the spectrum of Au@PtNCs from 3000 to 500 cm^{-1}. Meanwhile, the FTIR peaks for the detection antibodies and the immune Au@PtNCs around 2940 cm^{-1} corresponding to N−H stretch were found, which were not present in Au@PtNCs, also indicating the successful modification of the antibodies onto the Au@PtNCs. These results revealed that the detection antibodies were successfully modified onto the surface of Au@PtNCs through the electrostatic interaction and hydrophobic effect.

Optimization of the Proposed Biosensor. Both the pH value and the amount of detection antibodies have an impact on the conjugation of the detection antibodies with the Au@PtNCs. Thus, different pH values from 5.0 to 9.0 were used to prepare the immune Au@PtNCs for reacting with the target bacteria at 4.0×10^3 CFU/mL, and the absorbance at 652 nm was measured to optimize the pH value. As shown in Figure 4A, the absorbance increased rapidly from 0.31 to 0.59 when the pH value changed from 5.0 to 6.0 and decreased gradually to 0.21 when the pH value kept increasing to 9.0. Therefore, the optimal pH value of 6.0 was used for the preparation of the immune Au@PtNCs. In addition, different amounts of detection antibodies from 5 to 15 μg were employed to prepare the immune Au@PtNCs for detection of *Salmonella* at 4.0×10^3 CFU/mL. Figure 4B shows that the absorbance at

DOI: 10.1021/acssensors.9b01472
ACS Sens. 2020, 5, 65−72

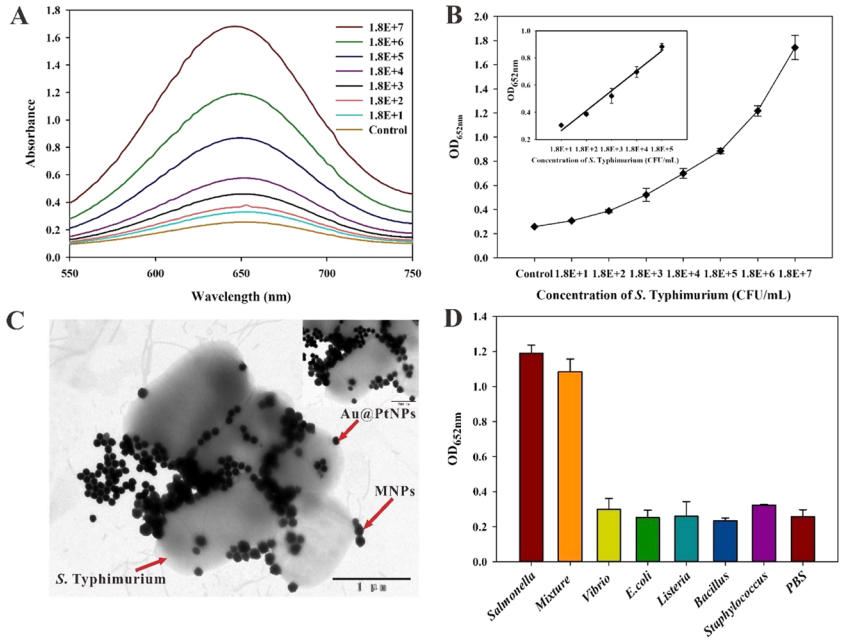

Figure 5. (A) Absorption spectra for different concentrations of bacteria; (B) calibration curve of the biosensor; (C) TEM image of MNP−bacteria−Au@PtNC complexes; (D) the specificity of the biosensor.

Table 1. Detection of *S. typhimurium* in Chicken Samples Using the Biosensor

	intra-assay			inter-assay[a]		
spiked *S. typhimurium* (CFU/mL)	detected[b] (CFU/mL)	recovery (%)	CV (%)	detected[b] (CFU/mL)	recovery (%)	CV (%)
57	63	110.58	6.48	62	109.48	10.51
570	553	96.93	8.45	492	86.29	7.98
5700	5054	88.67	6.01	6552	114.94	5.23

[a]Assay was conducted every day for three continuous days. [b]Mean value of five replicates at each concentration.

652 nm changed quickly from 0.36 to 0.66 when the amount of antibodies increased from 5 to 15 μg and did not increase significantly when more antibodies were used. This might be because 15 μg of the antibodies were sufficient for the modification of the Au@PtNCs. Thus, the optimal amount of 15 μg for the antibodies was used.

The amount of immune Au@PtNCs, the immunoreaction time, and the catalysis time are also important to the biosensor. Thus, different volumes of the immune Au@PtNCs were applied to detect the target bacteria (concentration: 4.0×10^3 CFU/mL). Figure 4C shows that the absorbance at 652 nm increased quickly from 0.13 to 0.60 when the volumes of the Au@PtNCs changed from 3 to 15 μL and decreased to 0.42 when more Au@PtNCs were used. This might be due to steric hindrance. Therefore, the optimal volume of 15 μL for Au@PtNCs was used. In addition, different immunoreaction times for the antibodies to conjugate with the target bacteria and different catalysis times for the Au@PtNCs to catalyze H_2O_2−TMB were both compared. Figure 4D shows that the absorbance changed from 0.28 to 0.68 when the immunoreaction time was increased from 0 to 30 min, and remained almost at the same level when the time kept increasing. Thus, the optimal time for the immunoreaction was 30 min. Figure 4E shows that the absorbance changed from 0.24 to 0.51 when the catalysis time was increased from 0 to 15 min, and remained at the same level after 15 min, meaning that 15 min was sufficient for Au@PtNCs to catalyze H_2O_2−TMB. Therefore, the optimal catalysis time was 15 min.

Sensitivity and Specificity of the Biosensor. Different concentrations of *S. typhimurium* from 1.8×10^1 to 1.8×10^7 CFU/mL were detected by the biosensor under optimal conditions. Figure 5A,B shows that the absorbance increased from 0.26 to 1.74 when the concentration changed from 1.8×10^1 to 1.8×10^7 CFU/mL. A good linear relationship between absorbance (A) and concentration (C) was obtained and could be described as $A = 0.0637 \ln(C) + 0.0819$ ($R^2 = 0.98$). The lower detection limit for the biosensor was calculated to be 17 CFU/mL based on three times signal-to-noise ratio. The biosensor had high sensitivity, which could be mainly ascribed to (1) the efficient immunoreaction of the antibodies with the target bacteria using the 3D fluidic chip to rapidly and sufficiently mix the solutions, which is the primary novelty of this study; (2) the effective amplification of the biological signal using the Au@PtNCs with high catalytic activity, better stability, and lower cost as a mimic enzyme to catalyze the H_2O_2−TMB substrate; and (3) the specific separation and enrichment of target bacteria using immune magnetic nanoparticles to capture the target bacteria. Meanwhile, the biosensor could complete the bacterial detection within 1 h. Besides, TEM imaging was conducted to demonstrate the formation of MNP−bacteria−Au@PtNC complexes (see Figure 5C).

The specificity of the biosensor was tested by detecting five other foodborne pathogens. The experimental results on the target bacteria (*S. typhimurium*), the nontarget bacteria (*V. parahaemolyticus*, *E. coli* O157: H7, *L. monocytogenes*, *B. cereus*,

DOI: 10.1021/acssensors.9b01472
ACS Sens. 2020, 5, 65−72

and *S. aureus*), and their mixture at 1.8×10^6 CFU/mL could be found in Figure 5D. The nontarget bacteria showed obviously lower absorbances (0.30 for *Vibrio*, 0.25 for *E. coli*, 0.26 for *Listeria*, 0.23 for *Bacillus*, and 0.32 for *Staphylococcus*) than the target *S. typhimurium* (1.19). In addition, the absorbance (1.10) for the mixture containing all bacteria was at a similar level to that for the target bacteria. These results demonstrated that the biosensor showed satisfactory specificity.

Applicability of the Biosensor in Real Food Sample Tests. To demonstrate the applicability of the biosensor, parallel tests on spiked chicken samples were performed. Both intra- and inter-assay were used to study the accuracy of the biosensor by testing three spiked chicken samples containing target bacteria from 5.7×10^1 to 5.7×10^3 CFU/mL. Intra-assay was conducted in one day with five replicates at each concentration, while inter-assay was conducted in three continuous days with five replicates at each concentration. Table 1 shows that the mean recovery for intra-assay ranged from 88.67 to 110.58% with standard deviation from 6.01 to 8.45%. The average recovery for inter-assay ranged from 86.29 to 114.94% with standard deviation from 5.23 to 10.51%. The intra- and inter-assay variations demonstrated that the biosensor exhibited good applicability for detection of *S. typhimurium*.

CONCLUSIONS

In this study, an optical biosensor based on porous gold@platinum nanocatalysts and a 3D fluidic chip was successfully demonstrated for fast and sensitive detection of *Salmonella*. This biosensor could detect target bacteria as low as 17 CFU/mL within 1 h. Compared with some recent reported studies on *Salmonella* detection (see Table S1), this optical biosensor showed comparable or better sensitivity and a shorter time. The 3D fluidic chip was demonstrated to have excellent mixing efficiency, and the Au@PtNCs were verified to have superior peroxidase-like enzymatic activity. The biosensor could be further improved to achieve fully automatic detection of *Salmonella* by integrating the catalytic reaction and colorimetric measurement onto a single chip and has the potential to be extended for detecting other bacteria using their specific antibodies for monitoring foodborne bacteria across multiple stages of food chains.

ASSOCIATED CONTENT

Supporting Information

The Supporting Information is available free of charge at https://pubs.acs.org/doi/10.1021/acssensors.9b01472.

COMSOL simulation on the passive micromixer; capture efficiency of *Salmonella*; comparison of 3D mixing with shaking and vortexing; UV−vis absorption spectra of AuNPs and Au@PtNCs; comparison of various methods for detection of *Salmonella* (PDF)

Mixing effect in the passive 3D mixer (Video S1) (MP4)

AUTHOR INFORMATION

Corresponding Author

*E-mail: jianhan@cau.edu.cn. Phone/Fax: +86-10-62737599.

ORCID

Jianhan Lin: 0000-0001-9458-1077

Notes

The authors declare no competing financial interest.

ACKNOWLEDGMENTS

This research was funded by the National Key Research and Development Program of China (2016YFD0500706) and Walmart Foundation (SA17031161).

REFERENCES

(1) Tourlousse, D. M.; Ahmad, F.; Stedtfeld, R. D.; Seyrig, G.; Tiedje, J. M.; Hashsham, S. A. A polymer microfluidic chip for quantitative detection of multiple water- and foodborne pathogens using real-time fluorogenic loop-mediated isothermal amplification. *Biomed. Microdevices* **2012**, *14*, 769−778.

(2) Ryan, U.; Hijjawi, N.; Xiao, L. Foodborne cryptosporidiosis. *Int. J. Parasitol.* **2018**, *48*, 1−12.

(3) Mangal, M.; Bansal, S.; Sharma, S. K.; Gupta, R. K. Molecular Detection of Foodborne Pathogens: A Rapid and Accurate Answer to Food Safety. *Crit. Rev. Food Sci. Nutr.* **2016**, *56*, 1568−1584.

(4) Wen, C. Y.; Hu, J.; Zhang, Z. L.; Tian, Z. Q.; Ou, G. P.; Liao, Y. L.; Li, Y.; Xie, M.; Sun, Z. Y.; Pang, D. W. One-step sensitive detection of *Salmonella typhimurium* by coupling magnetic capture and fluorescence identification with functional nanospheres. *Anal. Chem.* **2013**, *85*, 1223−1230.

(5) You, D. J.; Geshell, K. J.; Yoon, J. Y. Direct and sensitive detection of foodborne pathogens within fresh produce samples using a field-deployable handheld device. *Biosens. Bioelectron.* **2011**, *28*, 399−406.

(6) Sheikhzadeh, E.; Chamsaz, M.; Turner, A. P. F.; Jager, E. W. H.; Beni, V. Label-free impedimetric biosensor for *Salmonella typhimurium* detection based on poly[pyrrole-co-3-carboxyl-pyrrole] copolymer supported aptamer. *Biosens. Bioelectron.* **2016**, *80*, 194−200.

(7) Fronczek, C. F.; You, D. J.; Yoon, J. Y. Single-pipetting microfluidic assay device for rapid detection of Salmonella from poultry package. *Biosens. Bioelectron.* **2013**, *40*, 342−349.

(8) Chen, J.; Park, B. Effect of immunomagnetic bead size on recovery of foodborne pathogenic bacteria. *Int. J. Food Microbiol.* **2018**, *267*, 1−8.

(9) Wu, W.; Li, J.; Pan, D.; Li, J.; Song, S.; Rong, M.; Li, Z.; Gao, J.; Lu, J. Gold nanoparticle-based enzyme-linked antibody-aptamer sandwich assay for detection of *Salmonella typhimurium*. *ACS Appl. Mater. Interfaces* **2014**, *6*, 16974−16981.

(10) Chen, J.; Park, B. Label-free screening of foodborne Salmonella using surface plasmon resonance imaging. *Anal. Bioanal. Chem.* **2017**, 5455.

(11) Chen, Q.; Wang, D.; Cai, G.; Xiong, Y.; Li, Y.; Wang, M.; Huo, H.; Lin, J. Fast and sensitive detection of foodborne pathogen using electrochemical impedance analysis, urease catalysis and microfluidics. *Biosens. Bioelectron.* **2016**, *86*, 770−776.

(12) Matsumura, Y.; Enomoto, Y.; Takahashi, M.; Maenosono, S. Metal (Au, Pt) Nanoparticle-Latex Nanocomposites as Probes for Immunochromatographic Test Strips with Enhanced Sensitivity. *ACS Appl. Mater. Interfaces* **2018**, *10*, 31977−31987.

(13) Alamer, S.; Eissa, S.; Chinnappan, R.; Herron, P.; Zourob, M. Rapid colorimetric lactoferrin-based sandwich immunoassay on cotton swabs for the detection of foodborne pathogenic bacteria. *Talanta* **2018**, *185*, 275−280.

(14) Zhou, L.; Fang, S.; Liu, Y.; Yang, R.; Song, D.; Long, F.; Zhu, A. Universal and reusable hapten/antibody-mediated portable optofluidic immunosensing platform for rapid on-site detection of pathogens. *Chemosphere* **2018**, *210*, 10−18.

(15) Vaisocherová-Lísalová, H.; Víšová, I.; Ermini, M. L.; Špringer, T.; Song, X. C.; Mrázek, J.; Lamačová, J.; Scott Lynn, N.; Šedivák, P.; Homola, J. Low-fouling surface plasmon resonance biosensor for multi-step detection of foodborne bacterial pathogens in complex food samples. *Biosens. Bioelectron.* **2016**, *80*, 84−90.

DOI: 10.1021/acssensors.9b01472
ACS Sens. 2020, 5, 65−72

(16) Mester, P.; Wagner, M.; Rossmanith, P. Molecular Enrichment for Qualitative Molecular Pathogen Detection in Food. *Food Anal. Methods* **2018**, *11*, 1251−1256.
(17) Bu, S.; Wang, K.; Ju, C.; Wang, C.; Li, Z.; Hao, Z.; Shen, M.; Wan, J. Point-of-care assay to detect foodborne pathogenic bacteria using a low-cost disposable medical infusion extension line as readout and MnO_2 nanoflowers. *Food Control* **2019**, *98*, 399−404.
(18) Bu, T.; Huang, Q.; Yan, L.; Zhang, W.; Dou, L.; Huang, L.; Yang, Q.; Zhao, B.; Yang, B.; Li, T.; Wang, J.; Zhang, D. Applicability of biological dye tracer in strip biosensor for ultrasensitive detection of pathogenic bacteria. *Food Chem.* **2019**, *274*, 816−821.
(19) Xie, J.; Zhang, X.; Wang, H.; Zheng, H.; Huang, Y.; Xie, J. Analytical and environmental applications of nanoparticles as enzyme mimetics. *TrAC, Trends Anal. Chem.* **2012**, *39*, 114−129.
(20) Song, Y.; Xia, X.; Wu, X.; Wang, P.; Qin, L. Integration of platinum nanoparticles with a volumetric bar-chart chip for biomarker assays. *Angew. Chem., Int. Ed.* **2014**, *53*, 12451−12455.
(21) Wei, H.; Wang, E. Nanomaterials with enzyme-like characteristics (nanozymes): next-generation artificial enzymes. *Chem. Soc. Rev.* **2013**, *42*, 6060−6093.
(22) Savas, S.; Altintas, Z. Graphene Quantum Dots as Nanozymes for Electrochemical Sensing of Yersinia enterocolitica in Milk and Human Serum. *Materials* **2019**, *12*, No. 2189.
(23) Yang, Y.; Liu, Q.; Liu, Y.; Cui, J.; Liu, H.; Wang, P.; Li, Y.; Chen, L.; Zhao, Z.; Dong, Y. A novel label-free electrochemical immunosensor based on functionalized nitrogen-doped graphene quantum dots for carcinoembryonic antigen detection. *Biosens. Bioelectron.* **2017**, *90*, 31−38.
(24) Jiang, B.; Li, C.; Malgras, V.; Imura, M.; Tominaka, S.; Yamauchi, Y. Mesoporous Pt nanospheres with designed pore surface as highly active electrocatalyst. *Chem. Sci.* **2016**, *7*, 1575−1581.
(25) Fu, Q.; Wu, Z.; Du, D.; Zhu, C.; Lin, Y.; Tang, Y. Versatile Barometer Biosensor Based on Au@Pt Core/Shell Nanoparticle Probe. *ACS Sens.* **2017**, *2*, 789−795.
(26) Loynachan, C. N.; Thomas, M. R.; Gray, E. R.; Richards, D. A.; Kim, J.; Miller, B. S.; Brookes, J. C.; Agarwal, S.; Chudasama, V.; McKendry, R. A.; Stevens, M. M. Platinum Nanocatalyst Amplification: Redefining the Gold Standard for Lateral Flow Immunoassays with Ultrabroad Dynamic Range. *ACS Nano* **2018**, *12*, 279−288.
(27) Lin, X. Q.; Deng, H. H.; Wu, G. W.; Peng, H. P.; Liu, A. L.; Lin, X. H.; Xia, X. H.; Chen, W. Platinum nanoparticles/graphene-oxide hybrid with excellent peroxidase-like activity and its application for cysteine detection. *Analyst* **2015**, *140*, 5251−5256.
(28) Gao, Z.; Xu, M.; Lu, M.; Chen, G.; Tang, D. Urchin-like (gold core)@(platinum shell) nanohybrids: A highly efficient peroxidase-mimetic system for in situ amplified colorimetric immunoassay. *Biosens. Bioelectron.* **2015**, *70*, 194−201.
(29) Chen, X.; Zhang, S. 3D micromixers based on Koch fractal principle. *Microsyst. Technol.* **2018**, *24*, 2627−2636.
(30) Chen, C.; Mehl, B. T.; Munshi, A. S.; Townsend, A. D.; Spence, D. M.; Martin, R. S. 3D-printed Microfluidic Devices: Fabrication, Advantages and Limitations-a Mini Review. *Anal. Methods* **2016**, *8*, 6005−6012.
(31) Lin, C.-C.; Wang, J.-H.; Wu, H.-W.; Lee, G.-B. Microfluidic Immunoassays. *J. Assoc. Lab. Autom.* **2010**, *15*, 253−274.
(32) Hwang, Y.; Candler, R. N. Non-planar PDMS microfluidic channels and actuators: a review. *Lab Chip* **2017**, *17*, 3948−3959.
(33) Wu, J. W.; Xia, H. M.; Zhang, Y. Y.; Zhao, S. F.; Zhu, P.; Wang, Z. P. An efficient micromixer combining oscillatory flow and divergent circular chambers. *Microsyst. Technol.* **2019**, 2741.
(34) Chung, Y. C.; Hsu, Y. L.; Jen, C. P.; Lu, M. C.; Lin, Y. C. Design of passive mixers utilizing microfluidic self-circulation in the mixing chamber. *Lab Chip* **2004**, *4*, 70−77.
(35) Saggiomo, V.; Velders, A. H. Simple 3D Printed Scaffold-Removal Method for the Fabrication of Intricate Microfluidic Devices. *Adv. Sci.* **2015**, *2*, No. 1500125.
(36) Li, N.; Zhao, P.; Astruc, D. Anisotropic gold nanoparticles: synthesis, properties, applications, and toxicity. *Angew. Chem., Int. Ed.* **2014**, *53*, 1756−1789.
(37) Li, Y.; Tang, Z.; Prasad, P. N.; Knecht, M. R.; Swihart, M. T. Peptide-mediated synthesis of gold nanoparticles: effects of peptide sequence and nature of binding on physicochemical properties. *Nanoscale* **2014**, *6*, 3165−3172.
(38) Yuan, Z.; Lu, F.; Peng, M.; Wang, C. W.; Tseng, Y. T.; Du, Y.; Cai, N.; Lien, C. W.; Chang, H. T.; He, Y.; Yeung, E. S. Selective Colorimetric Detection of Hydrogen Sulfide Based on Primary Amine-Active Ester Cross-Linking of Gold Nanoparticles. *Anal. Chem.* **2015**, *87*, 7267−7273.
(39) Alam, A.; Kim, K.-Y. Mixing performance of a planar micromixer with circular chambers and crossing constriction channels. *Sens. Actuators, B* **2013**, *176*, 639−652.

DOI: 10.1021/acssensors.9b01472
ACS Sens. 2020, 5, 65−72